Water **2015**, *7*, 3243-3262; doi:10.3390/w7073243

OPEN ACCESS

water

ISSN 2073-4441
www.mdpi.com/journal/water

Article

Rainfall Variability in the Huangfuchuang Watershed and Its Relationship with ENSO

Thelma Dede Baddoo [1], Yiqing Guan [1,2], Danrong Zhang [1,2,*] and Samuel A. Andam-Akorful [3,4,*]

[1] State Key Laboratory of Hydrology-Water Resources and Hydraulic Engineering, Hohai University, Nanjing 210098, China; E-Mails: mzdede2010@gmail.com (T.D.B.); yiqingguan@hhu.edu.cn (Y.G.)
[2] College of Hydrology and Water Resources, Hohai University, Nanjing 210098, China
[3] School of Earth Sciences and Engineering, Hohai University, Nanjing 210098, China
[4] Department of Geomatic Engineering, Kwame Nkrumah University of Science and Technology, Private Mail Box, Kumasi, Ghana

* Authors to whom correspondence should be addressed; E-Mails: danrong_zhang@hhu.edu.cn (D.Z.); sa_andam@hhu.edu.cn (S.A.A.-A.); Tel.: +86-137-7067-2828 (D.Z.); +86-152-9550-6044 (S.A.A.-A.).

Academic Editor: Miklas Scholz

Received: 9 April 2015 / Accepted: 9 June 2015 / Published: 25 June 2015

Abstract: The impact of the El Niño-Southern Oscillation (ENSO) phenomenon within the Huangfuchuan watershed, one of the major first-order sub-basins in the middle region of the Yellow River, has not clearly been established. Consequently, the co-varying relationships between rainfall and El Niño/La Niña spanning the period 1954 to 2010 are investigated. Trends and step changes in annual rainfall are investigated with the Mann-Kendall and the distribution free cumulative sum (CUSUM) tests. Wavelet transforms are employed to perform spectral analysis of temporal variations in rainfall rates within the watershed. Cross wavelet and wavelet coherence transforms are used to study localized co-varying relationships between rainfall and ENSO index. Results from statistical tests indicate that rainfall in the Huangfuchuan watershed is declining, although not significantly. In addition, wavelet coherency and cross wavelet analysis, and comparison of the extracted dominant annual rainfall and 2–7 year ENSO signals demonstrate that ENSO events impact Huangfuchuan rainfall with El Niño corresponding to rainfall decline and La Niña to rainfall increment with a semiannual to annual lag.

Keywords: ENSO; Huangfuchuan; China; wavelet; precipitation; Yellow River

1. Introduction

The Yellow River, the second largest river in China and the sixth longest in the world is the most important freshwater resource for northern and north-western China, supporting about 107 million people [1–3]. The Yellow River has long been regarded as the "Mother River of China" because human inhabitants have existed in this region since prehistoric times, and, therefore, water shortage issues have experienced particular attention throughout the world [4,5]. Many studies have indicated that the Yellow River basin is dominated by decreasing precipitation, which may further deteriorate the stress conditions on water resources [2,6,7]. The source areas/regions of a river form its major tributaries, contributing to its flow. The Yellow River is divided into three major reaches; the upper, middle and lower reaches [8]. The middle reaches of the Yellow River basin contribute significantly to the total streamflow and sediment discharge of the Yellow River [9]. Zhang *et al.* [6] indicated that there is evidence of precipitation decline in the middle portion of the Yellow River basin, particularly in the Loess Plateau. The Huangfuchuan watershed is one of the most important source areas in the middle reach of the Yellow River [8,10]. Studies by Sui *et al.* [11] observed that long-term precipitation depth in the Huangfuchuan watershed had a decreasing trend. Additionally, Zhou *et al.* [12] demonstrated that the climate aridity in the Huangfuchuan watershed has increased in the recent three decades.

Precipitation is considered as the primary source of water in China and, therefore, most water resource projects are designed and implemented based on the historical pattern of water availability, quality, and demand, assuming a constant climate [7,13–15]. In addition, precipitation is the exclusive source of the Yellow River as the river flows through arid, semi-arid and semi-humid regions; its distribution and trend affect the water resources in this basin to a large extent [7]. Similarly, precipitation is a direct natural factor influencing runoff in the Huangfuchuan watershed due to its semi-arid climatic conditions. However, the distribution of precipitation is uneven, and, therefore, a better understanding of precipitation variability on basin and regional scales is of great significance to management of water resources by assisting in the implementation of proper water management policies for sustainable ecological conservation and environmental protection [14,16].

The El Niño-Southern Oscillation (ENSO) is in recent times recognized as the most prominent mode of climate variability that operates on seasonal-to-interannual time scales influencing hydrology in many parts of the world [17,18]. Through its effect on the global atmospheric circulation, ENSO influences patterns of temperature and precipitation, including extreme events such as, drought, floods, and tropical cyclones, in many regions of the world [18]. ENSO accounts for the largest contribution to interannual climate variability globally with a 2–7 year period [19–22]. The warm phase of ENSO, El Niño is associated with rising sea surface temperature (SST), while the atmospheric convection zones of the tropical Pacific expand and merge. On the other hand, La Niña, the cold phase of ENSO is associated with low SST near the equator, with atmospheric convection zones that are isolated from each other [23]. The influence of ENSO on rainfall variability in China has been the subject of many studies (e.g., [3,24–26]). Previous studies by Ropelewski and Halpert [27] showed that there is no steady

relationship between El Niño and rainfall over China as a whole. Hui *et al.* [28] also pointed out that the connection between mean summer precipitation and the preceding winter SST anomalies (ENSO) in China have weakened since the 1980s, making regional prediction much more difficult. However, Lau and Weng [25] stated that during the summer of 1997, southern China faced severe flooding, while northern China experienced one of the driest seasons on record, which can be linked to the 1997/98 strong El Niño event. Furthermore, Tong *et al.* [29] showed that El Niño activity is closely related to flood episodes in the lower and middle Yangtze catchments, whereas dry spells are associated with it in the upper catchment of the river. Major hydrological events on the other hand, tend to exhibit a spurious relationship with La Niña in the basin [29]. In addition, Ronghui and Yifang [30], Ding [31], Zhang *et al.* [32], in investigating the impacts of ENSO events on summer rainfall variability in northern China, reported a shortfall in summer rainfall during the El Niño development and maturity stages, whereas abundant rainfall was observed during the weakening phase of an El Niño event.

Rainfall deficits in the Yellow river have been linked to El Niño events [3,33]. Fu *et al.* [4] reported that, the average annual precipitation in the Yellow River basin in an El Niño year is less than that in a La Niña year. Additionally, Wang and Li [26] found that, there is a significant correlation between monthly precipitation of semiarid northern China and ENSO in the frequency bands of 2–3 years; in that, during ENSO years, rainfall was mostly below normal with some occurrences of drought in this region. Furthermore, Wang *et al.* [34] confirmed that ENSO events often resulted in decreased precipitation in the source regions of the Yellow River.

To the best of our knowledge, studies on ENSO influences on northern China have usually focused on the Yellow River basin as a whole, and not much on the sub-basins which form its major tributaries. In this study, we investigate the relationship between rainfall and ENSO in the Huangfuchuan watershed, an important sub-catchment in the middle region of the Yellow River. The Yellow River also spans from a semi-humid zone into an arid zone and, though we know the impacts of ENSO on the basin as a whole, this study goes ahead to study the impacts of ENSO on a sub-basin in the semi-arid zone of the Yellow River basin to determine if there is any difference and at what timescale. The question here is what is the relationship between ENSO and rainfall variability in the middle source regions of the Yellow River basin, and to what extent is this relationship; in terms of different timescales? The main objectives of this study, therefore, are: (a) to correlate the findings of other studies to the declining rainfall trend; (b) to examine the relationship and impact of ENSO events on rainfall variability in terms of timescales, on the Huangfuchuan, which is one of the major middle source sub-basins of the Yellow River in northern China over the period 1954 to 2010. To this end, the current study adopts exploratory data analysis (EDA) and wavelet transforms to investigate trends and variability in rainfall patterns over the Huangfuchuan basin. Wavelet analysis has found many uses in hydrology, because it provides an effective approach for hydrologic time series analysis by revealing characteristics under multi-temporal scales. This means that wavelet analysis demonstrates the scale contents of a signal and its variability in time [35–38]. Here, wavelet analysis was employed to investigate the variations in the dominant rainfall modes/signals with time in the Huangfuchuan watershed. Additionally, we study the co-varying relationships between rainfall over the basin and ENSO using cross wavelet and wavelet coherence analysis [39,40]. Cross wavelet and wavelet coherence analysis have been used in many studies to identify covariance and coherency in geophysical time series (see, e.g., [7,37,41–43]).

Following a brief introduction in Section 1, the arrangement of the rest of the paper is as follows. Section 2 gives an overview of the study area. Additionally, Section 3 describes the datasets and methodology used in the study and the results obtained are discussed in Section 4. Finally, the conclusions from the results are inferred in Section 5.

2. Study Area

The Huangfuchuan watershed is the drainage area covered by River Huangfu in the north of the Hekou-Longmen region located between longitudes 110°18′ E and 111°12′ E and latitudes 39°12′ N and 39°54′ N spanning a surface area of 3246 km^2 [16]. The river is 137 km long, a tributary and one of the most important source areas in the middle reach of the Yellow River originating from the transect of the Erdos Plateau and Loess Plateau in Northern China flowing from northwest to southeast into the Yellow River [8,11,44]. The watershed lies in the semi-arid climatic region in the northern Shaanxi province with the majority in the inner Mongolia region [11,45]. With a typical monsoon climate, the watershed has an average annual precipitation of 350 mm to 450 mm with more than 80% coming from June to September and a mean annual air temperature ranging from 6.9 and 9.7 °C [16,45,46]. The Huangfu River is representative of the "hill-gully" landscape of the northern Loess Plateau [45]. The Loess Plateau has a greatly varied and rolling surface with a large topographic relief, a deep layer of loess, a loose layer of soil, and a fragmented landform and sparse vegetation [11]. Due to this feature of the Loess Plateau, the soils are greatly susceptible to water and wind erosion making the Huangfuchuan watershed one of the main sources of sediments into the Yellow River [8,45]. The Huangfuchuan watershed is shown in Figure 1.

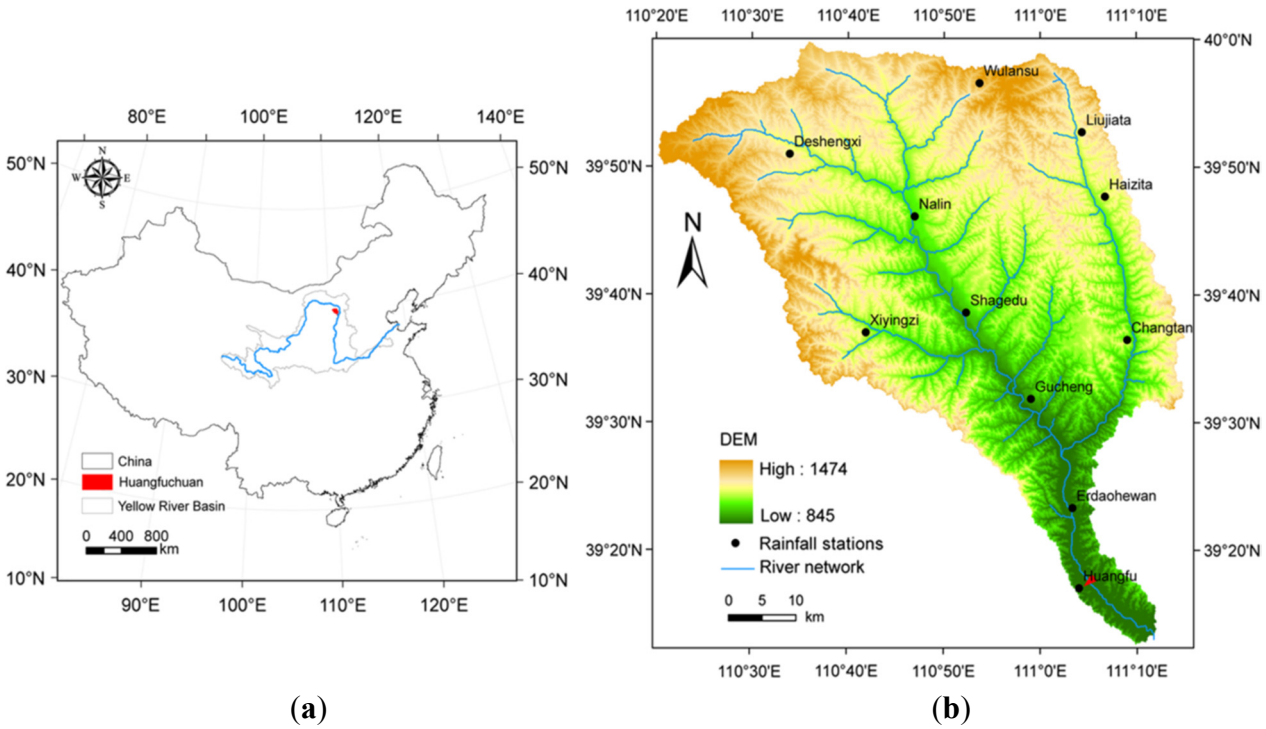

(**a**) (**b**)

Figure 1. Location of Huangfuchuan catchment in China (**a**) and the watershed map showing the different rainfall stations (**b**); the red arrow on the watershed map showing the hydrological station of the watershed. Retrieved from [47].

3. Materials and Methods

3.1. Materials

3.1.1. Rainfall data

Daily areal mean rainfall data from 1954 to 2010 was obtained from the "Experimental research on vegetation water source partitioning of riparian zone in arid and semi-arid areas based on multi-tracer technique and its uncertainty" (NSFC51209064) project taking place in the watershed. The daily rates were accumulated to monthly and annual rates for the purposes of this study.

3.1.2. Multivariate ENSO Index (MEI)

The Multivariate ENSO Index (MEI) time series was acquired from the Physical Sciences Division of the Earth System Research Laboratory of the National Oceanic and Atmospheric Administration (NOAA) at [48]. MEI is obtained as the first unrotated principal component (PC) of six variables over the tropical Pacific, which includes: sea-level pressure (P), zonal (U) and meridional (V) components of the surface wind, sea surface temperature (S), surface air temperature (A), and total cloudiness fraction of the sky (C). Given its multivariate nature, the index is claimed to provide a more vivid representation of characterizing the ENSO phenomenon relative to other indices, which only considers either the oceanic or atmospheric components [49]. It defines ENSO events as five consecutive overlapping three-month periods at or above the +0.5° anomaly for El Niño events and at or below the −0.5° anomaly for La Niña events. The strength of an event is further described as weak (with a 0.5 to 0.9 SST anomaly), moderate (1.0 to 1.4) and strong (≥1.5); an event is said to have occurred if the threshold is equaled or exceeded for at least three consecutive overlapping three-month periods. This study focuses only on strong and moderate El Niño/La Niña events. Figure 2 presents the MEI over the study period, showing the respective El Niño/La Niña events according to their strengths.

3.2. Methods

Annual precipitation values were calculated from the daily rainfall data of the Huangfuchuan watershed acquired. Exploratory data analysis was performed on the raw data to understand the data and have a summary of the visible patterns in rainfall in the watershed before applying statistical tests. Homogeneity tests were performed on the annual rainfall series to check the quality of the data. Four methods: standard normal homogeneity test (SNHT) [50], Buishand range test [51], Pettitt test [52], and von Neumann ratio test [53] were chosen to detect the homogeneity of the collected Huangfuchuan rainfall data. The test results are classified as: Useful (the series that rejects one or none null hypothesis under the four tests at 5% significance level), Doubtful (the series that rejects two null hypotheses of the four tests at 5% significance level) and Suspect (when there are three or all tests reject the null hypothesis at 5% significance level) as in [54,55]. The null hypothesis (H_0) in these tests assume that the data is homogeneous as opposed to the alternative hypothesis, H_a, that the series consists of a break in the mean. Distribution-free CUSUM (cumulative sum) test was employed to determine abrupt changes in rainfall patterns from 1954 to 2010 in the Huangfuchuan watershed. Similarly, the trend in the time series was established using the Mann-Kendall test statistic. The statistic software utilized was TREND

trend/change detection software, a product from the Cooperative Research Centre (CRC) for Catchment Hydrology's (CRCCH) Climate Variability Program [56]. Significance levels α = 0.01, 0.05 and 0.1 were used throughout.

Furthermore, wavelet power spectrum was employed to investigate the dominant cycles in rainfall pattern over the basin. Then, wavelet coherency (WTC) was used to identify where the two variables (rainfall and MEI) were correlated at a local scale. Furthermore, cross wavelet analysis (XWT) was adopted to investigate regions of high common power and further reveal information about the phase relationship of the two variables. The MatLab software package was used to perform all wavelet analysis. A MatLab software package for performing the XWT and WTC can be found at [57]. For more details on the wavelet analysis see [39].

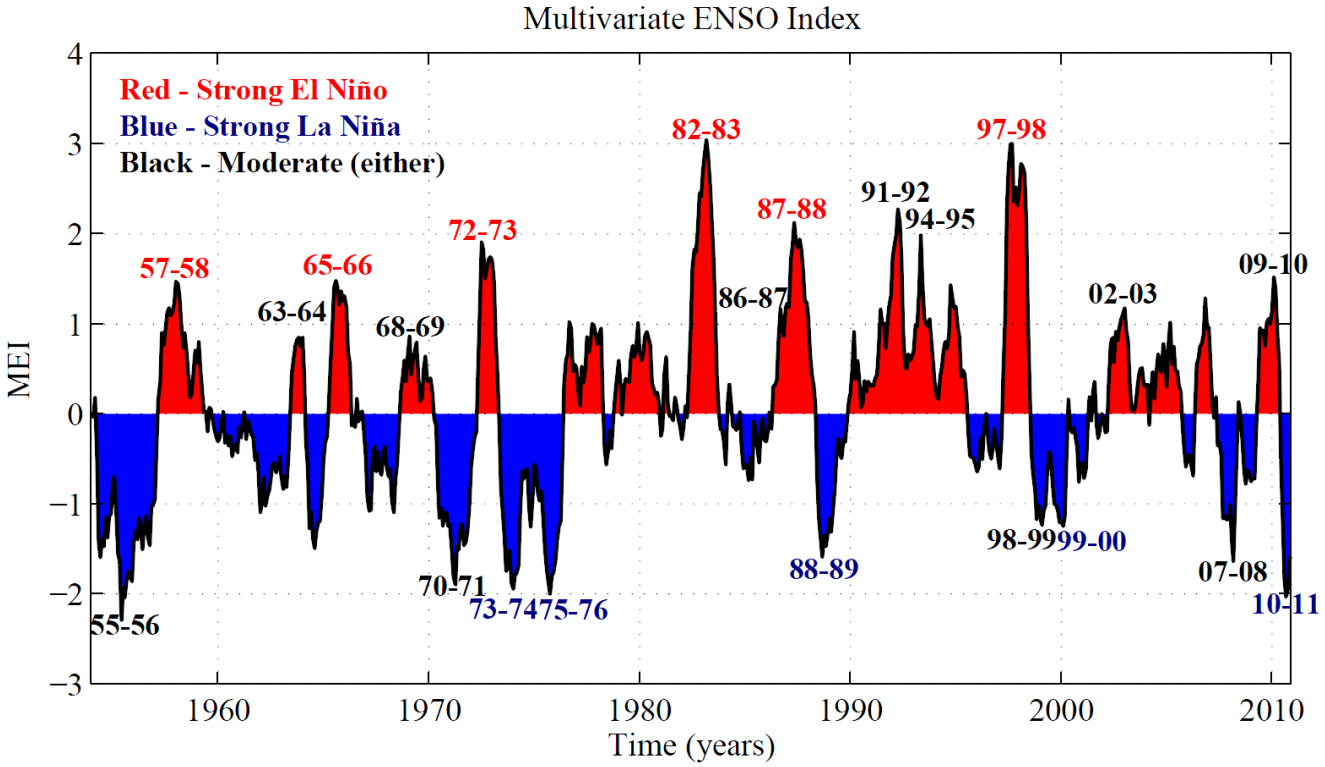

Figure 2. Multivariate ENSO indices from 1954 to 2010. El Niño (positive phase) in red; La Niña (negative phase) in blue. Numbers on the plot show El Niño/La Niña event years. Red and blue digits denote strong El Niño and La Niña events respectively. Black digits show the moderate years for either event.

3.2.1. Mann-Kendall Trend Analysis

This is a ranked nonparametric test developed by Mann [58] and Kendall [59]. The algorithm tests for monotonic trends and turning points in a series without a prior assumption of its distribution [60]. In this test, the null hypothesis H_0, assumes that the data is independent and arbitrarily ordered (that is, there is no trend and the observations are randomly ordered) and this is tested against the alternative hypothesis H_A, which assumes that there is a trend [61]. For details of the Mann-Kendall non-parametric test see [60].

3.2.2. Distribution Free Cumulative Sum (CUSUM) Test

This is a distribution free non-parametric test which determines whether the means in two parts of a record are different (for an unknown time of change) [56]. This rank-based test compares successive observations with the median of the series [62–64]. The test statistic V_k of a time series data is the maximum cumulative sum (CUSUM) of the signs of the difference from the median (a series of −1 or +1) starting from the beginning of the series [63,65]. More explanation on the distribution free CUSUM test can be found in [56].

3.2.3. Wavelet Analysis

The wavelet transform decomposes a series into time-frequency space, enabling the identification of both the dominant modes of variability and how those modes vary with time [66]. The wavelet transform as given by Labat [67] is:

$$W\left(\omega,\tau,x(t)\right)=\omega^{1/2}\int x(t)\Psi^{*}\left(\omega(t-\tau)\right)dt \quad (1)$$

where ω is the scale factor (frequency); τ is time shift; t is time; x(t) is the time series; and Ψ^{*} is the complex conjugate of Ψ, the wavelet function. The continuous wavelet transform is used in this study to compute the wavelet power spectrum. The Morlet wavelet function [68] given as

$$\Psi(t)=e^{-i\omega_0 t}e^{(-t^2/2)} \quad (2)$$

where $\Psi(t)$ is the wavelet function; i is the imaginary symbol of complex number; ω_0 is the non-dimensional frequency (ω_0= 6 to satisfy admissibility condition [69]); and t is time, was chosen as the mother-wavelet in this study because it describes the shape of hydrological signals well, and provides a good balance between time and frequency localization [67,70,71]. The standardized anomaly R'_{ij}, which removes seasonal fluctuations and short-term biases, was employed to standardize the rainfall data in the continuous wavelet transform and spectrum analysis according to

$$R'_{ij}=\frac{(R_{ij}-\overline{R}_j)}{\sigma_j} \quad (3)$$

where R_{ij} is the monthly averaged observed data in the year i and the month j, and $\overline{R}_j$ and σ_j represent the longterm mean and standard deviation of each successive month j, respectively [72]. For more details of wavelet transform analysis, see [67,73]. Figure 4 shows the wavelet analysis of total monthly Huangfuchuan precipitation intensity.

3.2.4. Cross Wavelet Spectrum

Cross-wavelet power reveals areas with a high common power [74]. According to Torrence and Compo [73], given two time series *X* and *Y*, with wavelet transforms $W_n^X(s)$ and $W_n^Y(s)$, where n is the time index and s is the scale, one can define the cross-wavelet spectrum as:

$$W_n^{XY}(s)=W_n^X(s)W_n^{Y*}(s) \quad (4)$$

where $W_n^{Y*}(s)$ is the complex conjugate of $W_n^Y(s)$. The cross-wavelet spectrum is complex, and hence one can define the cross-wavelet power as $|W_n^{XY}(s)|$. The phase angle of W_{XY} describes the phase relationship between X and Y in time-frequency space [39,40,75].

3.2.5. Wavelet Coherence

Wavelet coherence discussed refers to the Fourier squared coherency used to identify frequency bands within which two time series are co-varying [76]. The wavelet coherence (wavelet squared coherency) given by Torrence and Webster [76] is defined as the absolute value squared of the smoothed cross-wavelet spectrum, normalized by the smoothed wavelet power spectra,

$$\mathrm{R_n^2(s)} = \frac{|S(\mathrm{s^{-1}W_n^{XY}(s)})|^2}{S(\mathrm{s^{-1}}|\mathrm{W_n^X(s)}|^2).S(\mathrm{s^{-1}}|\mathrm{W_n^Y(s)}|^2)} \quad (5)$$

where S is a smoothing operator. Grinsted *et al.* [39] gives the smoothing operator as

$$S(W) = S_{scale}\left(S_{time}\left(W_n(s)\right)\right) \quad (6)$$

where S_{scale} denotes smoothing along the wavelet scale axis and S_{time} smoothing in time. For the Morlet wavelet, a suitable smoothing operator is given by Torrence and Webster [77] as

$$S_{time}(W)|_s = \left(W_n(s) * c_1^{\frac{-t^2}{2s^2}}\right)\Big|_s \quad (7)$$

$$S_{scale}(W)|_n = (W_n(s) * c_2 \Pi(0.6s))|_n \quad (8)$$

where c_1 and c_2 are normalization constants and Π is the rectangle function. The factor of 0.6 is the empirically determined scale decorrelation length for the Morlet wavelet [73]. The statistical significance level of the wavelet coherence is estimated using Monte Carlo methods [39]. Here, the wavelet coherence is used to identify both frequency bands and time intervals within which rainfall in the study area and ENSO are covarying.

4. Results and Discussion

4.1. Exploratory Data Analysis (EDA)

A quick look at the annual precipitation data values of the Huangfuchuan watershed (Figure 3) indicates that, the years before the 1970s recorded much more precipitation than the post 1970s. The annual rainfall amount in the watershed has decreased since 1968 until 2003. It can be seen that between 1968 and 2002, the basin experienced decreasing precipitation until a sharp rise in 2003. From 2003, annual precipitation decreased steeply till 2006 and rose sharply again in 2007 with another steep decline in 2009. The highest precipitation in the watershed occurred in 1959 and the lowest was 1999. The trend line indicates that rainfall intensity in the Huangfuchuan watershed decreased during the period of study. Furthermore, the equation of the linear trend line of Figure 3 demonstrates that rainfall in the Huangfuchuan watershed has been decreasing by 1.056 mm each year from 1954 to 2010.

Homogeneity test results on the annual rainfall data are presented in Table 1.

From Table 1, it is evident that the collected rainfall data is homogeneous and useful, and can therefore be used for further analysis.

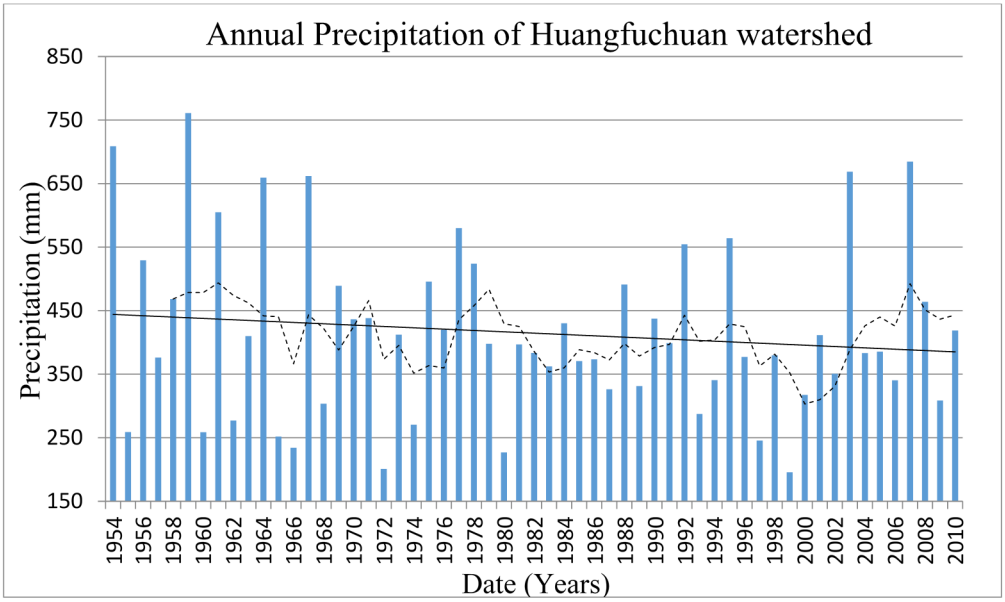

Figure 3. Annual precipitation of Huangfuchuan watershed. The dashed black line shows the five year moving average, while the straight black line shows the trend line.

Table 1. Homogeneity test results for annual rainfall data of the Huangfuchuan watershed.

Test Variables	SNHT	BR Test	Pettitt Test	VNR
Value	4.843	5.619	158.000	2.447
t (time of change)	1954	1964	1979	Does not determine time of change
p-value (two-tailed)	0.314	0.533	0.715	0.959
alpha (significance level)	0.05	0.05	0.05	0.05
Result	Accept the null hypothesis that the data is homogeneous	Accept the null hypothesis that the data is homogeneous	Accept the null hypothesis that the data is homogeneous	Accept the null hypothesis that the data is homogeneous

4.2. Statistical Analysis

The results of the Mann-Kendall statistical test performed on the annual rainfall time series of the Huangfuchuan watershed showed no statistically significant trend at $\alpha = 0.01$, 0.05 and 0.10. Although the trend is not significant, the negative value of the Z statistic shows a decreasing trend. This means that rainfall in the Huangfuchuan watershed is decreasing.

In addition, step change analysis from the distribution free CUSUM test on annual precipitation data showed no significant abrupt changes at significance levels of $\alpha = 0.01$, 0.05 and 0.1. Nevertheless, the results revealed a change point (year) in 1979 with a test statistic, V_k, of 8. The mean, median annual rainfall before and after 1979 were 439.6, 428.1 and 393.8, 379.8 respectively. Tables 2 and 3 summarize the statistical test results performed on the annual precipitation data of the Huangfuchuan watershed.

Table 2. Mann-Kendall test results of Huangfuchuan watershed.

S Statistic	Z	Critical Values			Interpretation
		α = 0.1	α = 0.05	α = 0.01	
−130	−0.888	1.645	1.96	2.576	NS

Notes: α = Significance level; NS = Not significant.

Table 3. Distribution free CUSUM test results.

Test Statistic (V_k)	Change Point (year)	Critical Values			Interpretation
		α = 0.1	α = 0.05	α = 0.01	
8	1979	9.211	10.268	12.306	NS

4.3. Wavelet Analysis

Figure 4 shows the results of wavelet analysis of monthly precipitation of Huangfuchuan watershed from 1954 to 2010.

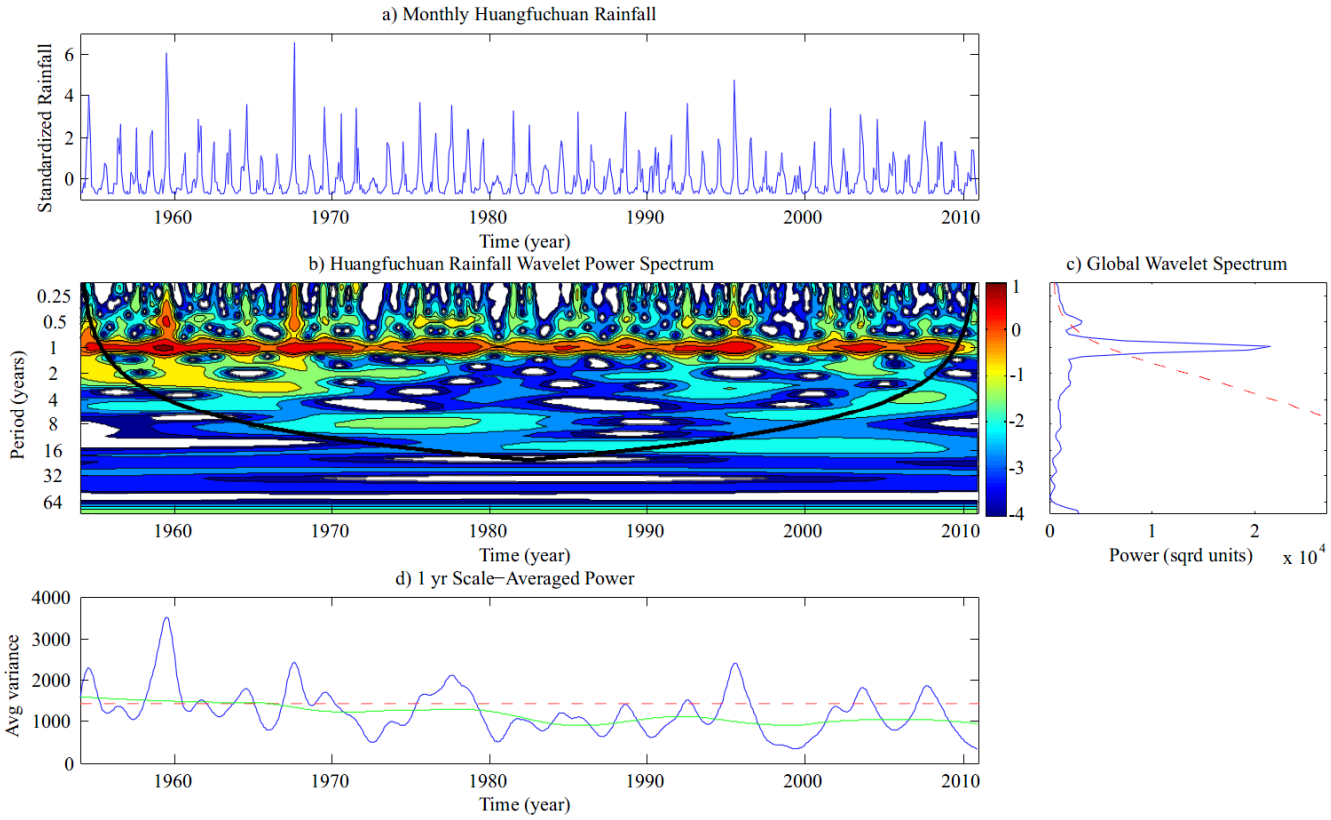

Figure 4. Wavelet analysis of monthly precipitation in the Huangfuchuan watershed; (**a**) is the standardized time series of precipitation; (**b**) is the wavelet power spectrum (WPS), the thick black arc delimits the cone of influence (COI) of the signal. High intensity is coded by the color red, whereas blue denotes the weaker intensity; (**c**) is the global wavelet spectrum for the WPS; and (**d**) is the averaged variance at the annual scale (blue). The dashed red line is the significant level. The green line shows the trend of the annual rainfall variance. Sqrd units indicates squared units.

From the global wavelet spectrum (Figure 4c), it is apparent that the dominant modes (highest intensity) of the precipitation signal is concentrated around the annual and semi-annual cycles, although the annual signal intensity is highest. The annual and semi-annual signals of 1959 have the highest power which corresponds to the high precipitation recorded in the region in that period. However, this above normal rainfall record corresponds to a four year lag after La Niña occurrence and a 17 month lag after an El Niño event in 1958, which suggests that the ENSO phenomenon may not have had a significant impact on rainfall during that period (see Figures 5a and 6). The low precipitation in 1999 also shows relatively high signal intensity. This rainfall decline was preceded by the strong 1997/98 El Niño event and an intermediate La Niña event in 1998, also in Figure 6. Annual signals for years 1960–1965, 1966–1971, 1974–1979, 1984–1985, 1988–1989, 1991–1996, 2001–2004, and 2006–2009 are analogous and relatively strong, whilst those between 1965–1966, 1971–1974, 1979–1984, 1985–1989, 1989–1991, 1996–2001 and 2005–2006 indicate lower amplitudes (see Figure 4). The relatively strong similar signals correspond to rainfall increment in average annual rainfall variance in Figure 4d. The contrast is true for lower amplitude signals. The averaged-annual scale power (Figure 4d) presents a persistent reduction in rainfall amplitudes between 1980 and 1994. There is a brief peak in 1996, after which the lowest amplitude is observed around 1997–1999. There seems to be a recovery in the amplitudes after this time, however, they are consistently below amplitudes observed before 1980. These results correspond to the following: between the periods of 1980 to 1999, there was a higher occurrence of El Niño events of higher intensities than the preceding years (see Figure 2). The recovery in rainfall amplitudes after 1999 occurred due to a reduction in the El Niño strengths in that period. However, the rainfall amplitudes in the recovery years were consistently below amplitudes before 1980 because, albeit the decline in El Niño strengths, its occurrence was greater than before the 1980s.

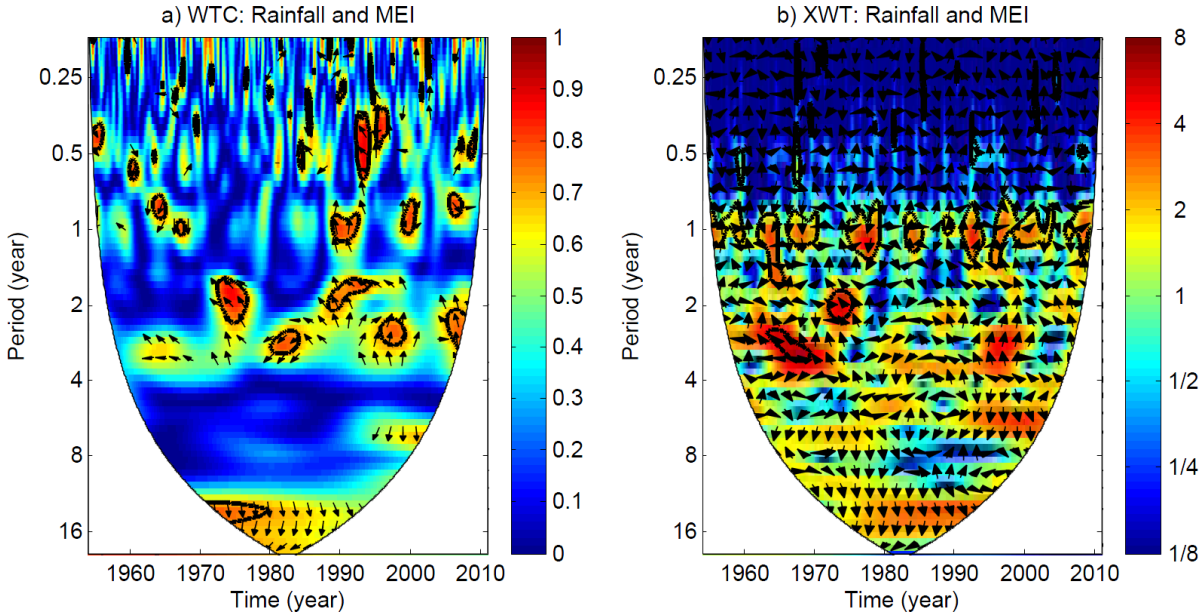

Figure 5. Wavelet coherency (**a**) and cross-wavelet spectrum (**b**) analysis showing the relations between Huangfuchuan rainfall and MEI. The thick black contour indicates the 95% confidence level against red noise and the cone of influence is shown as the lighter shade. The arrows (vectors) designate the phase difference between Huangfuchuan rainfall and MEI (with in-phase pointing right, anti-phase pointing left).

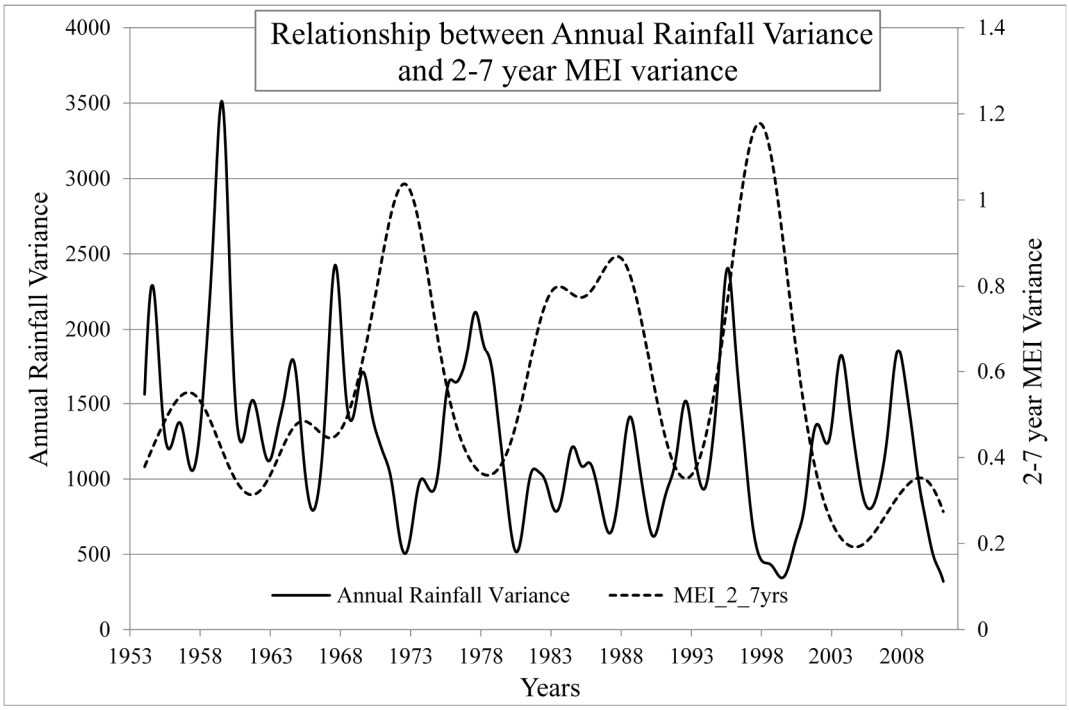

Figure 6. Relationship between Huangfuchuan rainfall and MEI showing the average annual rainfall variance and the 2–7 year variance of MEI. The black continuous curve shows rainfall and black dashed curve shows MEI.

Results of the co-varying relationships between rainfall and the ENSO phenomenon over the Huangfuchuan basin, as depicted by the wavelet coherence and cross wavelet are presented in Figure 5.

The wavelet coherence in Figure 5a shows significant covariance in the 0.5–1 year bands from 1954–1968. However; the significant sections within the semi-annual and annual (0.5–1 year) bands from 1954 to 1968 provide inadequate results concerning the phase difference of Huangfuchuan rainfall and MEI. Significant cross wavelet power of approximately 0.85 in the semi-annual (0.5) band from 1992 to 1994 shows an anti-phase difference of roughly 330° corresponding to rainfall deficit lagging an El Niño event. In addition, similar significant coherence in the same band from 1995 to 1997 corresponds to an approximate annual lag in rainfall with El Niño incidences inducing dry conditions. Additionally; a significant coherency of 0.8 in the annual band from 1988 to 1993 demonstrates an anti-phase difference of roughly 360°. This implies an annual lag of ENSO impacts on rainfall variability in the study watershed. Similarly significant covariance in the annual band from 1998 to 2001 indicates anti-phase difference of a year and more, corresponding to a rainfall deficit lagging the strong 1997/98 El Niño event by a year with persisting impacts. Furthermore, similarly significant coherence in the annual band during 2005 to 2008 does not provide adequate results on the phase difference. Looking at the ENSO frequency band (2–7 year band), significant coherence is also seen only around the 2–4 year band. The significant covariance of around 0.85 in the two year band from 1972–1977 indicates a 300° anti-phase difference correlating to induced dry periods lagging the 1972/73 El Niño event. This period also relates to a rainfall increase in 1977 preceded by successive strong La Niña events in 1973/74 and 1975/76. Significant coherence of around 0.75 within the two year band from 1988 to 1995 shows anti-phase difference of approximately 330° to 360° which can be linked to the 0.8 significant covariance in the annual band during approximately the same period (1988–1993). Additionally, significant covariance in the three year band

from 1980 to 1984 indicates a lag in rainfall deficit to El Niño events by approximately 240°. Moreover; similar coherency significance in the same band co-varies with about a 360° phase difference from 1996 to 2000 corresponding to an approximate annual lag in rainfall with El Niño occurrences inducing dry conditions. Likewise, the 0.75 significant covariance in the 2–4 year band from 2005 to 2008 correspond to an anti-phase difference of 11 to 12 months meaning rainfall lags ENSO events by that period. Finally, co-variance between Huangfuchuan rainfall and MEI within the ~14–16 year band from 1970 to 1980 shows anti-phase difference of 180° corresponding to a semi-annual lag in rainfall with ENSO events. This means that the seasonal impacts of ENSO on rainfall variability of the Huangfuchuan watershed occur on an annual scale, whereas, on a longer timescale; the impacts follow after six months and persist for a year or more. This result is representative of the fact that ENSO events usually occur in the boreal winter and the Huangfuchuan watershed experiences the majority of its rainfall in the summer (June; July and August) [16,78]. The persistence of the covariance from six months to a year can be attributed to the fact that ENSO signals can persist from one year to the next [79].

The cross-wavelet spectrum (XWT) of Huangfuchuan rainfall and MEI is shown in Figure 5b. It is noted that there is significant common power in the ~1–1.5 year band from 1955–1959, 1961–1970, 1974–1979, 1983–1986, 1988–1990, 1991–1994, 1995–2004 and 2005–2009. There is also highly significant common power in the 3–4 year band from 1963–1971 and in the 2 year band from 1972–1976. The arrows in the ~1–1.5 year band are randomly distributed and therefore, do not provide adequate results to conclude the phase difference of the two time periods. However, the arrows of the highly significant 2–4 year bands from 1963–1975 are relatively out of phase. That is the phase arrows in the two year band in the years 1972–1976 and the 3–4 year bands between 1963 and 1971 are ~300°–330° anti-phase meaning that the common power between the two time periods vary by 10 to 11 months. Figure 5b indicates that the two periods mainly have common power in the one-year band. The common power years in the one year band from 1955–1959 and 1974–1979 correspond to rainfall peaks in the study watershed. The rainfall peak from 1974–1979 correspond to strong La Niña events, whereas the ENSO-rainfall relationship from 1955–1959 are inconclusive. However, the common power years from 1961–1970, 1983–1986, 1988–1990, 1991–1994 and 1995–2004 mainly indicate troughs in the rainfall series corresponding to strong and intermediate El Niño events. The common power in the annual band from 2005–2009 also represents the recovery of rainfall in the study watershed correlating to intermediate El Niño events. This linkage is presented more clearly in Figure 6, which demonstrates the correlation between the ENSO events and rainfall in the Huangfuchuan catchment by extracting the 2–7 year and annual averaged variance respectively from the dominant modes of their wavelet analysis: 2–7 years for ENSO and annual (1 year) for rainfall.

Figure 6 illustrates the extracted dominant signals of rainfall in the Huangfuchuan watershed which is located at the annual scale and that of the Multivariate ENSO Index (MEI) which has been shown by [18–21] to be in the 2–7 year bands. Figure 6 is presented to further establish the relationship between annual Huangfuchuan rainfall and ENSO, or the modulating effects ENSO has on annual rainfall in the study watershed.

Figure 6 demonstrates that the warm tongue of the ENSO phenomenon (*i.e.*, El Niño) corresponds to rainfall decline, whereas the cold (La Niña) enhances rainfall. For examples, the strong 72/73, 87/88 and 97/98 El Niño events coincided with decreased rainfall amounts in the succeeding years; the 1997/98 event causing the driest period in the watershed [25]. The results of El Niño impacts on annual rainfall

in the Huangfuchuan basin are similar to that of La Niña, although, El Niño impacts are more pronounced. For the study period, no strong La Niña events occurred before the 1970s, though the moderate occurrence in 1955/56 caused a decline in rainfall in 1957. Subsequent La Niña occurrences result in increasing rainfall in the watershed from the 1970s. For example, the strong La Niña events of 73/74, 75/76, 88/89 and 99/00 resulted in increasing rainfall in the years 1975, 1977, 1990 and 2001, respectively. From the above observations, it can be presented that El Niño events have a greater influence on the Huangfuchuan watershed, relative to La Niña.

Furthermore, we performed correlation tests between rainfall and MEI, as well as the extracted annual rainfall and 2–7 year MEI variances to further investigate the relationship(s) between the two. To this end, both the Pearson linear and Spearman rank correlations were employed at a 0.05 significance level as presented in Table 4. The coefficients for the original series (*i.e.*, rainfall and MEI) exhibit weak relationships with varying signs for correlation methods (−0.050 and 0.028 respectively for Pearson and Spearman), which is expected since both fields are non-linear and non-stationary. However, for the extracted series, both methods yielded a stronger correlation with the same coefficient ($R = -0.363$), demonstrating the efficacy of wavelets to accurately represent the dominant patterns in non-linear, non-stationary series. The negative correlation indicates an anti-phase relationship between rainfall and ENSO phenomenon in the Huanfuchuan watershed, *i.e.*, El Nino results in dryer than normal conditions, whereas the converse is true for La Nina events. Moreover, we employed the proportion of variance explained (PVE) to quantify the magnitude of rainfall explained by the ENSO phenomenon in the Huanfuchuan watershed. The result suggests that ENSO events accounts for ~13% of Huangfuchuan rainfall, which implies that, other factors also impact rainfall variability in the watershed.

Table 4. Comparison of correlation results of unfiltered and filtered rainfall and multivariate El Niño-Southern oscillation index (MEI) data.

Data	Pearson Correlation	Spearman Rank Correlation
Monthly rainfall and MEI data (original)	−0.05	0.028
Extracted annual rainfall and 2–7 year MEI	−0.363	−0.363

Additionally, to further investigate the behavior of the rainfall-ENSO relationship during earlier years and more recent times, a Spearman rank correlation was performed for the extracted signals before and from 1968. The result is shown in Table 5. The correlation results of Table 5 shows that ENSO impacts on Huangfuchuan rainfall were more pronounced from 1968 than in earlier years. This supports the observation in Figure 6 showing the weak relationship between Huangfuchuan rainfall and ENSO events before 1968.

Table 5. Correlation results of rainfall-El Niño-Southern oscillation index (ENSO) relationship before and from 1968.

Extracted Annual Rainfall and 2–7 Year MEI	Spearman Rank Correlation
Before 1968	−0.113
From 1968	−0.351

5. Conclusions

In this study, wavelet analysis was employed to investigate the impact of ENSO events on the variability of precipitation in the Huangfuchuan watershed. The following points were concluded from the study:

(1) Results from the wavelet power spectrum presented an annual trend in Huangfuchuan rainfall. The Mann-Kendall trend test and the average annual variance of the wavelet analysis showed a downward trend in the annual rainfall amounts, although this trend was found to be statistically insignificant.

(2) Cross-wavelet transform analysis indicated that, Huangfuchuan rainfall is dominated by the 1–1.5 year band which has common powers corresponding to peaks and troughs in the rainfall time series. The phase difference arrows of the watershed rainfall and MEI in the 1–1.5 year bands for the cross-wavelet transform are randomly distributed and, therefore, do not provide adequate results to conclude the phase difference of the two time periods. However, significant common power in the 2–4 year band demonstrates that the common power of the two time periods varies by 10 to 11 months.

(3) Wavelet coherency results establish a six-month to one year phase difference between MEI and rainfall in the Huangfuchuan watershed. This means that ENSO events lead rainfall in the watershed by that period.

(4) The wavelet spectral analysis revealed that the dominant patterns in rainfall series are located at the annual scale, while that of the Multivariate ENSO Index (MEI) is found at the 2–7 year frequency band. The extracted signals at the dominant scales indicated that no significant relationship was identified between the two series (*i.e.*, rainfall and MEI) before 1968 while subsequent years demonstrated that ENSO events have a modulating effect on rainfall, especially during the El Niño activity, which induces dry conditions. The wavelet coherence analysis showed that rainfall lags ENSO by six to twelve months. A Pearson correlation and Spearman rank correlation analysis of the extracted signals of rainfall in the Huangfuchuan watershed and MEI further demonstrated that El Niño events correspond to recurring drought periods and La Niña events are succeeded by increases in rainfall.

Overall, ENSO events impact Huangfuchuan rainfall with El Niño corresponding to rainfall decline and La Niña to rainfall increase with a semiannual to annual lag. However, the impacts of El Niño persist in the watershed, resulting in increasing aridity in the study area. Other precipitation influences such as the intra-seasonal changes, Indian summer monsoons, and many others, coupled with anthropogenic factors, may be at play, when MEI events do not correlate with rainfall intensities.

Acknowledgments

This research paper is funded and supported by the National Natural Science Foundation of China (NSFC51209064).

Author Contributions

Yiqing Guan and Danrong Zhang were primarily responsible for data compilation and design and coordination of the study. Thelma Dede Baddoo and Samuel A. Andam-Akorful were responsible for data analysis, interpretation and writing of the paper.

Conflicts of Interest

The authors declare no conflict of interest.

References

1. McVicar, T.R.; Van Niel, T.G.; Li, L.; Hutchinson, M.F.; Mu, X.; Liu, Z. Spatially distributing monthly reference evapotranspiration and pan evaporation considering topographic influences. *J. Hydrol.* **2007**, *338*, 196–220.
2. She, D.; Xia, J. The spatial and temporal analysis of dry spells in the Yellow River basin, China. *Stoch. Environ. Res. Risk Assess.* **2012**, *27*, 29–42.
3. Wang, H.; Yang, Z.; Saito, Y.; Liu, J.P.; Sun, X. Interannual and seasonal variation of the Huanghe (Yellow River) water discharge over the past 50 years: Connections to impacts from ENSO events and dams. *Glob. Planet. Chang.* **2006**, *50*, 212–225.
4. Fu, G.; Charles, S.P.; Viney, N.R.; Chen, S.; Wu, J.Q. Impacts of climate variability on stream-flow in the Yellow River. *Hydrol. Process.* **2007**, *21*, 3431–3439.
5. Wang, R.; Ren, H.; Ouyang, Z. China water vision. In *Foreign Language Book*; China Meteorological Press: Beijing, China, 2000.
6. Zhang, Q.; Peng, J.; Singh, V.P.; Li, J.; Chen, Y.D. Spatio-Temporal variations of precipitation in arid and semiarid regions of China: The Yellow River basin as a case study. *Glob. Planet. Chang.* **2014**, *114*, 38–49.
7. Liu, Q.; Yang, Z.; Cui, B. Spatial and temporal variability of annual precipitation during 1961–2006 in Yellow River Basin, China. *J. Hydrol.* **2008**, *361*, 330–338.
8. Yellow River Conservancy Commission. *Assessment Report of Climate Change Impact and Water Resources of the Yellow River Basin*; UNESCO Office Beijing: Beijing, China, 2009.
9. Zhao, G.; Tian, P.; Mu, X.; Jiao, J.; Wang, F.; Gao, P. Quantifying the impact of climate variability and human activities on streamflow in the middle reaches of the Yellow River basin, China. *J. Hydrol.* **2014**, *519*, 387–398.
10. Zhou, Y.; Yang, Z.; Zhang, D.; Jin, X.; Zhang, J. Inter-Catchment comparison of flow regime between the Hailiutu and Huangfuchuan rivers in the semi-arid Erdos Plateau, NW China. *Hydrol. Sci. J.* **2015**, *60*, 688–705.
11. Sui, J.; He, Y.; Karney, B.W. Flow and high sediment yield from the Huangfuchuan watershed. *Int. J. Environ. Sci. Technol.* **2008**, *5*, 149–160.
12. Zhou, Y.; Shi, C.; Fan, X.; Shao, W. The influence of climate change and anthropogenic activities on annual runoff of Huangfuchuan basin in northwest China. *Theor. Appl. Climatol.* **2015**, *120*, 137–146.
13. Abdul Aziz, O.I.; Burn, D.H. Trends and variability in the hydrological regime of the Mackenzie

River Basin. *J. Hydrol.* **2006**, *319*, 282–294.
14. Liang, L.; Li, L.; Liu, Q. Precipitation variability in Northeast China from 1961 to 2008. *J. Hydrol.* **2011**, *404*, 67–76.
15. Westmacott, J.R.; Burn, D.H. Climate change effects on the hydrologic regime within the Churchill-Nelson River Basin. *J. Hydrol.* **1997**, *202*, 263–279.
16. Li, E.; Mu, X.; Zhao, G.; Gao, P.; Shao, H. Variation of runoff and precipitation in the hekou-longmen region of the yellow river based on elasticity analysis. *Sci. World J.* **2014**, *2014*, doi: 10.1155/2014/929858.
17. Ward, P.J.; Jongman, B.; Kummu, M.; Dettinger, M.D.; Sperna Weiland, F.C.; Winsemius, H.C. Strong influence of El Nino Southern Oscillation on flood risk around the world. *Proc. Natl. Acad. Sci. USA* **2014**, *111*, 15659–15664.
18. Zebiak, S.E.; Orlove, B.; Muñoz, Á.G.; Vaughan, C.; Hansen, J.; Troy, T.; Thomson, M.C.; Lustig, A.; Garvin, S. Investigating El Niño-Southern Oscillation and society relationships. *Wiley Interdiscip. Rev. Clim. Chang.* **2015**, *6*, 17–34.
19. Bellenger, H.; Guilyardi, E.; Leloup, J.; Lengaigne, M.; Vialard, J. ENSO representation in climate models: From CMIP3 to CMIP5. *Clim. Dyn.* **2014**, *42*, 1999–2018.
20. Dai, A. The influence of the inter-decadal Pacific oscillation on US precipitation during 1923–2010. *Clim. Dyn.* **2013**, *41*, 633–646.
21. Donders, T.H.; Punyasena, S.W.; de Boer, H.J.; Wagner-Cremer, F. ENSO signature in botanical proxy time series extends terrestrial El Niño record into the (sub)tropics. *Geophys. Res. Lett.* **2013**, *40*, 5776–5781.
22. Zebiak, S.E. Air-Sea interaction in the equatorial Atlantic region. *J. Clim.* **1993**, *6*, 1567–1586.
23. Philander, S.G.H. El Niño and La Niña. *J. Atmos. Sci.* **1985**, *42*, 2652–2662.
24. Feng, S.; Hu, Q. Variations in the teleconnection of ENSO and summer rainfall in Northern China: A role of the Indian Summer Monsoon. *J. Clim.* **2004**, *17*, 4871–4881.
25. Lau, K.M.; Weng, H. Coherent modes of global SST and summer rainfall over China: An assessment of the regional impacts of the 1997–98 El Niño. *J. Clim.* **2001**, *14*, 1294–1308.
26. Wang, W.-C.; Li, K. Precipitation fluctuation over semiarid region in northern China and the relationship with El Nino/Southern Oscillation. *J. Clim.* **1990**, *3*, 769–783.
27. Ropelewski, C.F.; Halpert, M.S. Global and regional scale precipitation patterns associated with the El Niño/Southern Oscillation. *Mon. Weather Rev.* **1987**, *115*, 1606–1626.
28. Hui, G.; Yongguang, W.; Jinhai, H. Weakening significance of ENSO as a predictor of summer precipitation in China. *Geophys. Res. Lett.* **2006**, *33*, L09807.
29. Tong, J.; Qiang, Z.; Deming, Z.; Yijin, W. Yangtze floods and droughts (China) and teleconnections with ENSO activities (1470–2003). *Quat. Int.* **2006**, *144*, 29–37.
30. Ronghui, H.; Yifang, W. The influence of ENSO on the summer climate change in China and its mechanism. *Adv. Atmos. Sci.* **1989**, *6*, 21–32.
31. Ding, Y. *Monsoons over China*; Springer Science & Business Media: Dordrecht, The Netherlands, 1994; Volume 16.
32. Zhang, R.; Sumi, A.; Kimoto, M. A diagnostic study of the impact of El Niño on the precipitation in China. *Adv. Atmos. Sci.* **1999**, *16*, 229–241.

33. Kiem, A.S.; Geogievsky, M.V.; Hapuarachchi, H.P.; Ishidaira, H.; Takeuchi, K. Relationship between ENSO and snow covered area in the Mekong and Yellow River basins. In Proceedings of the International Symposium on Regional Hydrological Impacts of Climatic Variability and Change with an Emphasis on Less Developed Countries, Held during the 7th Scientific Assembly of the International Association of Hydrological Sciences, Foz de Iguaço, Brazil, 3–9 April 2005; Volume 2, pp. 255–264.
34. Wang, G.X.; Shen, Y.P.; Liu, S.Y. On the characteristics of response of precipitation and runoff to the ENSO events in the source regions of the Yellow River. *J. Glaciol. Geocryol.* **2001**, *23*, 16–21.
35. Sang, Y.-F. A review on the applications of wavelet transform in hydrology time series analysis. *Atmos. Res.* **2013**, *122*, 8–15.
36. Maheswaran, R.; Khosa, R. Comparative study of different wavelets for hydrologic forecasting. *Comput. Geosci.* **2012**, *46*, 284–295.
37. Sang, Y.-F. Improved Wavelet Modeling Framework for Hydrologic Time Series Forecasting. *Water Resour. Manag.* **2013**, *27*, 2807–2821.
38. Hao, Y.; Liu, G.; Li, H.; Li, Z.; Zhao, J.; Jim Yeh, T.-C. Investigation of karstic hydrological processes of Niangziguan Springs (North China) using wavelet analysis. *Hydrol. Process.* **2012**, *26*, 3062–3069.
39. Grinsted, A.; Moore, J.C.; Jevrejeva, S. Application of the cross wavelet transform and wavelet coherence to geophysical time series. *Nonlinear Process. Geophys.* **2004**, *11*, 561–566.
40. Jevrejeva, S.; Moore, J.C.; Grinsted, A. Influence of the Arctic Oscillation and El Niño-Southern Oscillation (ENSO) on ice conditions in the Baltic Sea: The wavelet approach. *J. Geophys. Res.* **2003**, *108*, doi:10.1029/2003JD003417.
41. Lin, Y.-C.; Yu, H.-L. The cross wavelet and wavelet coherence analysis of spatio-temporal rainfall-groundwater system in Pingtung plain, Taiwan. In Proceedings of the EGU General Assembly 2013, Vienna, Austria, 7–12 April 2013; Volume 15.
42. Shanahan, T.M.; Overpeck, J.T.; Anchukaitis, K.J.; Beck, J.W.; Cole, J.E.; Dettman, D.L.; Peck, J.A; Scholz, C.A; King, J.W. Atlantic forcing of persistent drought in West Africa. *Science* **2009**, *324*, 377–380.
43. Yin, Y.; Xu, Y.; Chen, Y. Relationship between flood/drought disasters and ENSO from 1857 to 2003 in the Taihu Lake basin, China. *Quat. Int.* **2009**, *208*, 93–101.
44. Xu, H.; Taylor, R.; Kingston, D.; Thompson, J.; Todd, M. Impact of climate scenarios on water resources in River Xiangxi and Huangfuchuan basin. In Proceedings of the Quest-GSI Water Resources Workshop, Reading, UK, 30 March–3 April 2009.
45. Xu, H.; Taylor, R.G.; Xu, Y. Quantifying uncertainty in the impacts of climate change on river discharge in sub-catchments of the Yangtze and Yellow River Basins, China. *Hydrol. Earth Syst. Sci.* **2011**, *15*, 333–344.
46. Li, T.; Wang, G.; Huang, Y.; Fu, X. Response of soil erosion and sediment yield to the temporal variation of precipitation in the Loess Plateau. In Proceedings of the 15th International Congress of the International Soil Conservation Organization (ISCO); Budapest, Hungary, 18–23 May 2008.
47. Tian, P.; Zhao, G.; Mu, X.; Wang, F.; Gao, P.; Mi, Z. Check dam identification using multisource data and their effects on streamflow and sediment load in a Chinese Loess Plateau catchment. *J. Appl. Remote Sens.* **2013**, *7*, doi:10.1117/1.JRS.7.073697.

48. NOAA/OAR/ESRL PSD Multivariate ENSO Index (MEI). Available Online: http://www.esrl.noaa.gov/psd/enso/mei/ (accessed on 15 October 2014).
49. Wolter, K.; Timlin, M.S. El Niño/Southern Oscillation behaviour since 1871 as diagnosed in an extended multivariate ENSO index (MEI.ext). *Int. J. Climatol.* **2011**, *31*, 1074–1087.
50. Alexandersson, H. A homogeneity test applied to precipitation data. *J. Climatol.* **1986**, *6*, 661–675.
51. Buishand, T.A. Some methods for testing the homogeneity of rainfall records. *J. Hydrol.* **1982**, *58*, 11–27.
52. Pettitt, A.N. A non-parametric approach to the change-point problem. *Appl. Stat.* **1979**, 126–135.
53. Von Neumann, J. Distribution of the ratio of the mean square successive difference to the variance. *Ann. Math. Stat.* **1941**, *12*, 367–395.
54. Wijngaard, J.B.; Klein Tank, A.M.G.; Können, G.P. Homogeneity of 20th century European daily temperature and precipitation series. *Int. J. Climatol.* **2003**, *23*, 679–692.
55. Kang, H.; Yusof, F. Homogeneity tests on daily rainfall series in Peninsular Malaysia. *Int. J. Contemp. Math. Sci.* **2012**, *7*, 9–22.
56. Chiew, F.; Siriwardena, L. *Trend User Guide 2005*; CRC for Catchment Hydrology: Canberra, Australia, 2005.
57. NOC/NERC Crosswavelet and Wavelet Coherence. Available Online: http://noc.ac.uk/using-science/crosswavelet-wavelet-coherence (accessed on 3 September 2014).
58. Mann, H.B. Nonparametric tests against trend. *Econom. J. Econom. Soc.* **1945**, 245–259.
59. Kendall, M.G. *Rank Correlation Measures*; Charles Griffin: London, UK, 1975; Volume 202.
60. Mondal, A.; Kundu, S.; Mukhopadhyay, A. Rainfall trend analysis by Mann-Kendall test: A case study of north-eastern part of Cuttack District, Orissa. *Int. J. Geol. Earth Environ. Sci.* **2012**, *2*, 70–78.
61. Onoz, B.; Bayazit, M. The power of statistical tests for trend detection. *Turkish J. Eng. Environ. Sci.* **2003**, *27*, 247–251.
62. Chiew, F.H.S.; McMahon, T.A. Detection of trend or change in annual flow of Australian rivers. *Int. J. Climatol.* **1993**, *13*, 643–653.
63. Kundzewicz, Z.W.; Robson, A. (Eds) *Detecting Trend and Other Changes in Hydrological Data*; WCDMP-46, WMO/TD-No.1025; World Meteorological Organization (WMO): Geneva, Switzerland, 2000.
64. McGilchrist, C.A.; Woodyer, K.D. Note on a distribution-free CUSUM technique. *Technometrics* **1975**, *17*, 321–325.
65. Karpouzos, D.K.; Kavalieratou, S.; Babajimopoulos, C. Trend analysis of precipitation data in Pieria Region (Greece). *Eur. Water* **2010**, *30*, 31–40.
66. Kim, S. Wavelet analysis of precipitation variability in northern California, U.S.A. *KSCE J. Civ. Eng.* **2004**, *8*, 471–477.
67. Labat, D. Recent advances in wavelet analyses: Part 1. A review of concepts. *J. Hydrol.* **2005**, *314*, 275–288.
68. Morlet, J.; Arens, G.; Fourgeau, E.; Glard, D. Wave propagation and sampling theory-Part I: Complex signal and scattering in multilayered media. *Geophysics* **1982**, *47*, 203–221.
69. Farge, M. Wavelet transforms and their applications to turbulence. *Annu. Rev. Fluid Mech.* **1992**, *24*, 395–457.

70. Gaucherel, C. Use of wavelet transform for temporal characterisation of remote watersheds. *J. Hydrol.* **2002**, *269*, 101–121.
71. Kang, S.; Lin, H. Wavelet analysis of hydrological and water quality signals in an agricultural watershed. *J. Hydrol.* **2007**, *338*, 1–14.
72. Nakken, M. Wavelet analysis of rainfall-runoff variability isolating climatic from anthropogenic patterns. *Environ. Model. Softw.* **1999**, *14*, 283–295.
73. Torrence, C.; Compo, G.P. A practical guide to wavelet analysis. *Bull. Am. Meteorol. Soc.* **1998**, *79*, 61–78.
74. Zhang, Q.; Xu, C.; Jiang, T.; Wu, Y. Possible influence of ENSO on annual maximum streamflow of the Yangtze River, China. *J. Hydrol.* **2007**, *333*, 265–274.
75. Jevrejeva, S.; Moore, J.C.; Grinsted, A. ENSO signal propagation detected by wavelet coherence and mean phase coherence methods. In *Nonlinear Dynamics in Geosciences*; Tsonis, A.A.; Elsner, J.B., Eds.; Springer New York: New York, NY, USA, 2007; pp. 167–175.
76. Torrence, C.; Webster, P.J. Interdecadal Changes in the ENSO–Monsoon System. *J. Clim.* **1999**, *12*, 2679–2690.
77. Torrence, C.; Webster, P.J. The annual cycle of persistence in the El Nño/Southern Oscillation. *Q. J. R. Meteorol. Soc.* **1998**, *124*, 1985–2004.
78. Rasmusson, E.M.; Carpenter, T.H. Variations in tropical sea surface temperature and surface wind fields associated with the Southern Oscillation/El Niño. *Mon. Weather Rev.* **1982**, *110*, 354–384.
79. Wu, R.; Hu, Z.-Z.; Kirtman, B.P. Evolution of ENSO-related rainfall anomalies in East Asia. *J. Clim.* **2003**, *16*, 3742–3758.